Adaptive High-Order Discontinuous Galerkin Solution of Elastohydrodynamic Lubrication Point Contact Problems

H Lu [a], M Berzins [b], CE Goodyer [c], PK Jimack [c,*],

[a] *College of Aerospace Engineering, Nanjing University of Aeronautics and Astronautics, Nanjing, China, 210016*

[b] *Scientific Computing and Imaging Institute, University of Utah, USA*

[c] *School of Computing, University of Leeds, LS2 9JT, UK*

Abstract

This paper describes an adaptive implementation of a high order Discontinuous Galerkin (DG) method for the solution of elastohydrodynamic lubrication (EHL) point contact problems. These problems arise when modelling the thin lubricating film between contacts which are under sufficiently high pressure that the elastic deformation of the contacting elements cannot be neglected. The governing equations are highly nonlinear and include a second order partial differential equation that is derived via the thin-film approximation. Furthermore, the problem features a free boundary, which models where cavitation occurs, and this is automatically captured as part of the solution process. The need for spatial adaptivity stems from the highly variable length scales that are present in typical solutions. Results are presented which demonstrate both the effectiveness and the limitations of the proposed adaptive algorithm.

Preprint submitted to Elsevier Science *10 October 2011*

Key words: Elastohydrodynamic lubrication, Discontinuous Galerkin, High polynomial degree, h-adaptivity, Nonlinear systems

1 Introduction

In order to minimize power loss and to prevent wear caused by friction lubricants are used to separate machine components that would otherwise be in contact. The behaviour of the lubricating film is of great importance in determining its performance and has therefore been a topic of considerable research over many years, from [28,5] through to the present day [17,18]. In many cases, in particular when the pressure is sufficiently high compared to the stiffness of the contacting surfaces, the elastic deformation of these surfaces cannot be ignored since it has a significant effect on the behaviour and properties of the lubricant film. Such a situation is referred to as Elastohydrodynamic Lubrication (EHL). Examples of the occurrence of EHL include cases where a very large force is applied over a very small surface area, such as in journal bearings and gears [31], or cases where the contacting elements are relatively easily deformed, such as in bio-mechanics [4]. In many of these situations it is difficult to undertake reliable measurement through physical experiments since, for example, the lubricant film may be very thin and the pressure in the contact region may be extremely high (up to 3GPa) [20].

* Corresponding author.
Email addresses: hongqiang.lu@nuaa.edu.cn (H Lu), mb@sci.utah.edu (M Berzins), c.e.goodyer@leeds.ac.uk (CE Goodyer), p.k.jimack@leeds.ac.uk (PK Jimack).

Historically, two common models have been applied to describe lubricated contact problems: line and point models. In both cases, dimensional reduction of the problem is achieved via the application of a thin film approximation, which allows the Navier-Stokes equations to be simplified to equations involving just pressure and film thickness (known as the Reynolds and the film thickness equations). In the case of a line contact further dimensional reduction is achieved by neglecting end effects and just modelling the cross-section of the contact. In this paper, we are concerned with point-contact problems, which we will model locally by the flow of a lubricating film between a plane surface and a paraboloid (which may deform). One of the typical features of EHL solutions is the existence of a sharp ridge of high pressure on the outflow of the point contact. (For line contact problems this is referred to as a pressure spike or the "Petrusevich spike" after the work of Petrusevich [28] who was the first to compute numerical solutions for an EHL line contact problem.)

Up until very recently the most widely used techniques for the solution of EHL problems have been based upon the use of low order finite difference methods combined with multigrid techniques. Multigrid was first employed to accelerate convergence by Lubrecht in 1986 [26]. Furthermore, for the fast calculation of the elastic deformation Brandt and Lubrecht [2] developed a multilevel multi-integration algorithm which significantly reduces the computational complexity in approximating deformations at each point in the contact. Venner [34,33] contributed further improvements on relaxation robustness. This combination of finite difference discretizations and a multi-level solver combines both efficiency and stability even when a very large number of degrees of freedom are required. However the approach is somewhat inflexible since it does not accommodate high order or locally refined approximations very naturally, meaning

that very large numbers of degrees of freedom are typically required in order to obtain accurate solutions [13,24,12]. In recent years therefore interest in the use of finite element methods and more tightly coupled approaches has increased, initially with work such as [6,19,8], and more recently using higher order continuous elements [15,16].

In this paper we propose a new numerical technique for the solution of two-dimensional, point contact, EHL problems based upon the use of a high order Discontinuous Galerkin (DG) discretization combined with automatic adaptive refinement. The approach is a generalization and extension of the technique introduced by the authors in [24] for lower dimensional line contact problems. In addition to generalizing the DG solution algorithm to two space dimensions, including using of a penalty method [37] to handle the potentially complex free boundary, this paper also demonstrates the importance of spatial adaptivity. In particular, results are included that show the millions of degrees of freedom required for two-dimensional multi-level finite difference approximations (see [12]) can be reduced to just thousands of degrees of freedom using adaptive DG.

In the following section the governing equations for the EHL point contact are introduced and in Section 3 their DG discretization is discussed. Section 4 describes the solution of the resulting system of highly nonlinear algebraic equations, including the use of p-multigrid techniques. Section 5 discusses the spatial adaptivity in detail as the use of a discontinuous approximation significantly simplifies the mesh refinement in two dimensions which is thus fully exploited in the proposed algorithm. Section 6 provides an overview of the whole solution procedure before the paper concludes with a description of a number of computational examples, followed by a short discussion.

2 Governing Equations

The dimensionless mathematical model used in this work to describe isothermal EHL problems consists of three equations: the Reynolds equation, which is derived from a thin-film approximation of the fluid flow; the film thickness equation (based upon a linear elastic deformation model for the solid contact elements), and a force balance equation [29,34]. The non-dimensional steady-state Reynolds equation may be written in the following form:

$$- \bigtriangledown \cdot(\epsilon \bigtriangledown P) + \bigtriangledown \cdot (\beta \rho H) = 0, \tag{1}$$

where $\beta = (1, 0)$ for a model point contact (reflecting an assumed inflow of the lubricant from the negative x-axis). Here P is the non-dimensional pressure, which is the active variable, H is the non-dimensional film thickness and ρ is the non-dimensional density of the lubricant. Further,

$$\epsilon = \frac{\rho H^3}{\eta \lambda}, \tag{2}$$

where η is the viscosity of the lubricant and λ a dimensionless speed parameter, which assumed constant for this steady-state model. Note that ϵ is small in the contact region and relatively large in the non-contact region, which leads to the fact that the diffusion term of the Reynolds equation (1) dominates in the non-contact region and the convection term dominates in the contact region. This has to be carefully considered when performing discretization and relaxation.

The film thickness equation, which defines the contact geometry for a given pressure solution, takes the following form:

$$H(x,y) = H_{00} + \frac{x^2}{2} + \frac{y^2}{2} + \frac{2}{\pi^2}\int_{-\infty}^{\infty}\int_{-\infty}^{\infty}\frac{P(x',y')}{\sqrt{(x-x')^2+(y-y')^2}}\,\mathrm{d}x'\mathrm{d}y'. \tag{3}$$

This commonly used approximation, e.g. [2,12,26,33], is derived from the analytic solution to the linear elasticity problem on a semi-infinite domain, where H_{00} is the central offset film thickness (a constant of integration), the parabolic term represents the undeformed point contact geometry (assumed circular in this case), and the global integral describes the elastic deformation itself.

The force balance equation is a conservation law for the applied load. For a non-dimensional point contact, it is given by:

$$\int_{-\infty}^{\infty}\int_{-\infty}^{\infty} P(x,y)\,\mathrm{d}x\mathrm{d}y - \frac{2\pi}{3} = 0. \tag{4}$$

In practice, the lubricant rheology is highly non-linear in pressure and so, in this work, the following viscosity-pressure relationship of Roelands [34] is assumed:

$$\eta(P) = e^{\{\frac{\alpha p_0}{z}[-1+(1+\frac{Pp_h}{p_0})^z]\}}, \tag{5}$$

where $z = 0.68$ is the viscosity index, $\alpha = 2.165\times10^{-8}$ is the pressure-viscosity index, and $p_0 = 1.98\times10^8$ is ambient pressure. The density model of Dowson and Higginson (see [34]) is used to describe the compressibility of the lubricant:

$$\rho(P) = \frac{0.59\times10^9 + 1.34Pp_h}{0.59\times10^9 + Pp_h}, \tag{6}$$

where p_h is the maximum Hertzian pressure which is a known constant for any given loaded case. Whilst certainly not unique, these viscosity and density models are widely used throughout the EHL literature [11,34].

All two dimensional EHL solutions can be characterized in terms of the di-

mensionless point contact parameters W, U and G (or Moes dimensionless parameters M and L) [34] where W is a dimensionless load parameter, U is a dimensionless speed parameter and G is a material parameter. Given W, U and G, M and L can be calculated as:

$$M = W(2U)^{-0.75}, \tag{7}$$

$$L = G(2U)^{0.25}. \tag{8}$$

Then p_h in equations (5) and (6) and λ in equation (2) can be evaluated as follows:

$$p_h = \frac{(\frac{3}{2}M)^{\frac{1}{3}}L}{\pi\alpha}, \tag{9}$$

$$\lambda = (\frac{128\pi^3}{3M^4})^{\frac{1}{3}}. \tag{10}$$

Note that equation (1) only defines the non-dimensional pressure, P, to within an arbitrary constant so, without loss of generality, we are able to define the vapour pressure of the lubricant to be zero (this is enforced through the upstream boundary condition). However, the solution of the Reynolds equation allows the pressure in the outlet region to decrease without limit if the outlet boundary is too far from the contact region. Consequently, the location of the outlet boundary should be treated as free so as to ensure that $P > 0$, so cavitation does not occur, within the domain itself. These boundary constraints may be expressed as:

$$P(X_{boundary}) = 0, \quad \text{and} \quad \hat{n} \cdot \bigtriangledown P(X_{boundary}) = 0, \tag{11}$$

where $\hat{n}$ is the unit normal to the boundary and $X = (x, y)$ in 2d. The inlet boundary should be located to approximate an infinite upstream boundary.

3 High-Order Discontinuous Galerkin Discretization

This section describes the high-order DG discretization of the three governing equations (1), (3) and (4).

3.1 The Reynolds Equation

Let $\mathcal{P}_h$ be a partition of the domain Ω into N rectangular elements Ω_e (each with boundary $\partial\Omega_e$). Moreover, let $\Gamma_{int} = \cup\Gamma_{ef}$ where Γ_{ef} represents each internal interface,

$$\Gamma_{ef} = \partial\Omega_e \cap \partial\Omega_f \tag{12}$$

with $e > f$, and let $\hat{n}$ be the unit normal pointing outward from Ω_e. Finally let Γ_D be the boundary of Ω, which is taken to be a Dirichlet boundary where $P = g$. Further let Γ_- be the inflow part of the boundary, which is the part of Γ_D for which $\hat{n}\cdot\beta < 0$, where $\hat{n}$ is the outward normal from the computational domain. Here g is the solution on the Dirichlet boundary and for all problems considered in this paper $g = 0$, which is reasonable so long as the upstream and span-wise boundaries are sufficiently far from the contact region (see Figure 1 for an illustration of the finite computational domain).

The jump of a function v at point X on the element interface Γ_{ef} is defined to be

$$[v]_{ef}(X) = v(X)|_{\partial\Omega_e\cap\Gamma_{ef}} - v(X)|_{\partial\Omega_f\cap\Gamma_{ef}},\ e > f, \tag{13}$$

and the average is given by

$$\langle v(X)\rangle_{ef} = \frac{1}{2}(v(X)|_{\partial\Omega_e\cap\Gamma_{ef}} + v(X)|_{\partial\Omega_f\cap\Gamma_{ef}}). \tag{14}$$

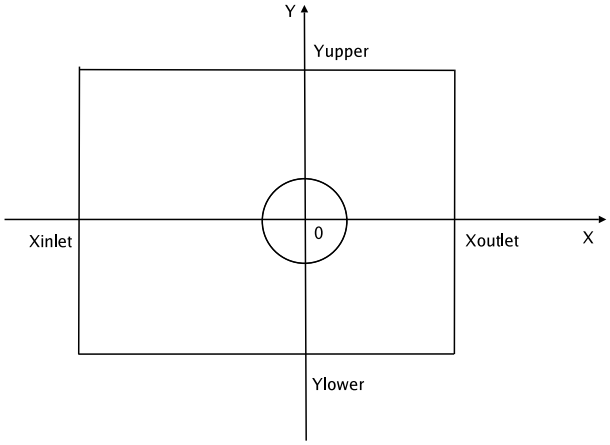

Fig. 1. Computational domain used for the DG discretization of equations (1, 3, 4)

In each element, P is expressed in the following form:

$$P^e(X) = \sum_{i=1}^{n(p^e)} u_i^e N_i^e(X), \tag{15}$$

where p^e is the degree of the approximating polynomial, $n(p^e)$ is the number of the basis functions required to achieve this order on each element, u_i^e are the unknown coefficients and $N_i^e(X)$ are the local finite element basis functions which span a finite element space V. In this paper, *hierarchical* basis functions are used, based on the definitions in [32]. Briefly, these consist of "nodal modes", "edge modes" and "internal modes".

Following the approach of [1,27], a discrete form of the Reynolds equation becomes:

$$L(P, v) = a(P, v) - l(P, v) = 0, \ \forall v \in V \tag{16}$$

where

$$\begin{aligned} a(P, v) = & \sum_{\Omega_e \in \mathcal{P}_h} \left(\int_{\Omega_e} \bigtriangledown v \cdot \epsilon \bigtriangledown P \, \mathrm{d}X \right) \\ & + \int_{\Gamma_{int}} \left([P] \langle (\epsilon \bigtriangledown v) \cdot \hat{n} \rangle - [v] \langle (\epsilon \bigtriangledown P) \cdot \hat{n} \rangle \right) \mathrm{d}s \\ & + \int_{\Gamma_D} \left(P(\epsilon \bigtriangledown v) \cdot \hat{n} - v(\epsilon \bigtriangledown P) \cdot \hat{n} \right) \mathrm{d}s, \end{aligned} \tag{17}$$

and

$$l(P,v) = \sum_{\Omega_e \in \mathcal{P}_h} \left(\int_{\Omega_e} (\bigtriangledown v \cdot \beta) \rho H \, \mathrm{d}X \right) - \int_{\partial\Omega_e \setminus \Gamma_-} v(\rho(P^-)H)(\beta \cdot \tilde{n}_e) \, \mathrm{d}s$$
$$- \int_{\Gamma_-} v\rho(g)H(\beta \cdot \hat{n}) \, \mathrm{d}s + \int_{\Gamma_D} (\epsilon \bigtriangledown v) \cdot \hat{n} g \, \mathrm{d}s. \tag{18}$$

Note that these expressions imply the weak enforcement of the Dirichlet boundary conditions $P = g$ (where $g \equiv 0$ throughout this paper). Furthermore,

$$P^- = \lim_{\delta \to 0} P(X - \delta\beta), \text{ for } X \in \Gamma_{int}, \tag{19}$$

$\tilde{n}_e$ is the outward-pointing normal from Ω_e and, on Γ_D and $\hat{n}$ is the outward unit normal on Γ_D. Equation (19 is based upon [1] and represents the implementation of a form of upwinding, through the choice of P^-, when calculating the numerical flux over element boundaries in (18). The numerical results presented later in this paper are consistent with other applications of such an upwinded DG scheme, e.g. [1], in that it remains stable, at least for the low to moderately-loaded cases that we consider here.

3.2 The Film Thickness Equation

For a given pressure distribution the film thickness may be calculated as follows:

$$H(x,y) = H_{00} + \frac{x^2}{2} + \frac{y^2}{2}$$
$$+ \frac{2}{\pi^2} \int_{Y_{lower}}^{Y_{upper}} \int_{X_{inlet}}^{X_{outlet}} \frac{P(x',y')}{\sqrt{(x-x')^2 + (y-y')^2}} \, \mathrm{d}x' \mathrm{d}y'$$
$$= H_{00} + \frac{x^2}{2} + \frac{y^2}{2} + \frac{2}{\pi^2} \sum_{e=1}^{N} \sum_{i=1}^{n(p^e)} K_i^e(x,y) u_i^e, \tag{20}$$

where

$$K_i^e(x,y) = \int_{\Omega_e} \frac{N_i^e(x',y')}{\sqrt{(x-x')^2+(y-y')^2}}\,\mathrm{d}x'\,\mathrm{d}y'. \tag{21}$$

Here $K_i^e(x,y)$ is calculated using numerical quadrature. Special care must be taken when $(x,y) \in \Omega_e$ due to the singular nature of the integrand, and so singular quadrature [7] should be used. Gaussian quadrature can be employed elsewhere. Note that any error caused by the numerical quadrature when calculating these kernels would affect the accuracy of the film thickness, which has significant impact on the accuracy of the pressure through the convection term in the Reynolds equation. Therefore, when using either singular quadrature or Gaussian quadrature, $K_i^e(x,y)$ needs to be calculated sufficiently accurately. In this paper, adaptive quadrature is therefore used.

When using quadrature to evaluate the integrals over elements and element boundaries in equations (17) and (18), the value of the film thickness needs to be calculated at each quadrature point in each element and on each element boundary. In order to do this, the values of $K_i^e(x,y)$ must be evaluated at each quadrature point. Note however that, for a given grid, a given set of basis functions, and a given set of quadrature points, these kernels, $K_i^e(x,y)$, need only be evaluated once. This fact may be used to allow enormous efficiency gains to be made in the solution procedure. Note however that a large amount of memory is required to store the values of these kernels. If we have N elements and M edges in the computational domain and m-point quadrature is used, there will be $(N \times m^2 + M \times m) \times \sum_{e=1}^{N} n(p^e)$ double precision values to store.

The discrete form of the force balance equation is given by:

$$\sum_{e=1}^{N} \int_{\Omega_e} \sum_{i=1}^{n(p^e)} u_i^e N_i^e(x,y)\,\mathrm{d}x\mathrm{d}y - \frac{2\pi}{3} = 0. \tag{22}$$

Hence it is possible to define another kernel by

$$G_i^e = \int_{\Omega_e} N_i^e(x,y)\,\mathrm{d}x\mathrm{d}y, \tag{23}$$

to yield the following form:

$$\sum_{e=1}^{N} \sum_{i=1}^{n(p^e)} G_i^e u_i^e - \frac{2\pi}{3} = 0. \tag{24}$$

Again this kernel can be precomputed for a given grid and a given set of basis functions.

3.4 Penalty Method

A major issue that must be addressed by any numerical method for the solution of EHL problems is the treatment of the cavitation boundary. Recall from Section 2 that the Reynolds equation is only valid in regions for which it yields a non-negative pressure and the region in which it becomes zero is unknown *a priori*. A variety of techniques have been proposed for addressing this issue. In [36], for example, any non-positive pressures are simply set to zero (however the resulting model is clearly dependent upon the choice of the computational domain). More sophisticated (and accurate) approaches involve adapting the position of the outflow boundary as the computation of the solution values progresses [13,24]. In this paper, we use a penalty method that is based upon the approach used in [17,25,37]. This significantly simplifies the

treatment of the free boundary without appearing to lead to any significant loss of accuracy. The consequence of introducing an exterior penalty term [37] is to modify the discrete system (16) so that it becomes:

$$L(P,v) = a(P,v) + \frac{1}{\delta}\int_{\Omega} P_{-}v \,\mathrm{d}X - l(P,v) = 0, \ \forall v \in V, \tag{25}$$

where δ is an arbitrary small positive number ($\delta = 1.0\times10^{-7}$ in the calculations used in this paper) and

$$P_{-} = min(P,0). \tag{26}$$

Note that the penalty term $\frac{1}{\delta}\int_{\Omega} P_{-}v \,\mathrm{d}X$ is only effective when $P < 0$, in which case it dominates the equation (25) since δ is very small. In this case, the negative pressures are forced to be almost zero by the presence of the penalty term in the modified weak form. The physical constraint that $P \geq 0$ over the entire computational domain is then effectively satisfied automatically (negative pressures of $O(\delta)$ may still be present however).

4 Solution of the Discrete System

For EHL problems, solution of the resulting discrete system is always a challenge because the Reynolds equation (1) is a highly nonlinear equation due to ρ, H and η all depending on the active variable P. Furthermore, since the convection term of the Reynolds equation (1) dominates in the contact region and the diffusion term dominates elsewhere, any iterative method needs to be robust and efficient in both regions. In this paper, a nonlinear smoother for 2d steady-state EHL problems is developed, which is then combined with a multi-level algorithm based upon p-multigrid [9]. We begin this section with a description of the single level solver and then extend this to incorporate

p-multigrid.

4.1 Relaxation

Substituting the expression (15) into (16)-(19) and using the basis functions as the test functions, the steady-state equation (25) can be written in the general nonlinear form:

$$L(U) = A(U)U - b(U) = 0, \tag{27}$$

where

$$U = (u_1^1, \ldots, u_{n(p^1)}^1; \ldots; u_1^N, \ldots, u_{n(p^N)}^N). \tag{28}$$

Note that both $A(U)$ and $b(U)$ depend upon U. Since the entries of U are ordered element by element, $A(U)$ is a sparse block matrix with non-zero blocks on the diagonal and non-zero off-diagonal blocks for block row e and block column f whenever e and f are neighbours (since each element e is connected with its neighbouring elements through the element boundaries, see equation (17)).

A simple iterative procedure for solving this nonlinear algebraic system is to use the following quasi-Newton relaxation:

$$U \leftarrow U - \left(\frac{\partial \hat{L(U)}}{\partial U} \right)^{-1} L(U), \tag{29}$$

where $\frac{\partial \hat{L(U)}}{\partial U}$ is an approximation to the true Jacobian $\frac{\partial L(U)}{\partial U}$:

$$\frac{\partial L(U)}{\partial U} = \frac{\partial (A(U)U)}{\partial U} - \frac{\partial b(U)}{\partial U} \approx A(U) - \frac{\partial b(U)}{\partial U}. \tag{30}$$

Note that $\frac{\partial b(U)}{\partial U}$ is a full matrix which can itself be approximated by:

$$\frac{\partial b(U)}{\partial U}|_{I,J} = \frac{\partial b(U)_i^e}{\partial U_j^f}$$
$$\approx \sum_{\Omega_e \in \mathcal{P}_h} \left(\int_{\Omega_e} (\bigtriangledown v \cdot \beta) \rho \frac{\partial H}{\partial U_j^f} \, \mathrm{d}X \right)$$
$$- \int_{\partial\Omega_e \setminus \Gamma_-} v(\rho(P^-) \frac{\partial H}{\partial U_j^f} + \frac{\partial \rho(P^-)}{\partial U_j^f} H)(\beta \cdot \hat{n}_e) \, \mathrm{d}s$$
$$- \int_{\Gamma_-} v\rho(g) \frac{\partial H}{\partial U_j^f} (\beta \cdot \hat{n}) \, \mathrm{d}s, \tag{31}$$

where the Ith row corresponds to the row generated with the test function $v = N_i^e(X)$ and the Jth column corresponds to the unknown U_j^f. Note that, according to the discrete film thickness equation (20),

$$\frac{\partial H(x,y)}{\partial U_j^f} = K_j^f(x,y), \tag{32}$$

which can be precomputed. However, by (20), the film thickness depends heavily on the local pressures and much less on the pressures far away. Thus, in (32), $K_j^f(x,y)$ is small when the position of element f is far away from the position of $X = (x,y)$. This provides useful information with which to make a further simplification to the approximation of $\frac{\partial b(U)}{\partial U}$. In (31) we use the following approximations:

(1) $\frac{\partial H(X)}{\partial U_j^f} = 0$ where $X \in e$ if $f \neq e$ and f is not a neighbour of e.
(2) $\frac{\partial H(X)}{\partial U_j^f} = 0$ where $X \in \Gamma_{int}$ if f is not a neighbour of Γ_{int}.
(3) $\frac{\partial H(X)}{\partial U_j^f} = 0$ where $X \in \Gamma_D$ if f is not a neighbour of Γ_D.
(4) $\frac{\partial H(X)}{\partial U_j^f} = K_j^f(X)$, otherwise.

Note that these approximations are of the simplest possible form and could be improved by taking into account the distance of point X from element f, rather than simply neglecting all non-neighbouring contributions.

The above principles lead to an approximation of $\frac{\partial b(U)}{\partial U}$ by a block sparse ma-

trix with the same sparsity as $A(U)$. As a result, $\frac{\partial \hat{L(U)}}{\partial U}$ in (29) is also a block sparse matrix. An advantage of this simplification is that it is only necessary to evaluate a relatively small number of the entries of $\frac{\partial b(U)}{\partial U}$ instead of calculating all of them (of course this may have an impact of the performance of the relaxation (29), especially for heavily loaded cases). Consequently, when updating the unknown U in (29), the following linear system is solved numerically rather than calculating $\left(\frac{\partial L(U)}{\partial U}\right)^{-1}$ precisely:

$$\frac{\partial \hat{L(U)}}{\partial U} U_{correction} = -L(U), \tag{33}$$

where U is the current solution, $\frac{\partial \hat{L(U)}}{\partial U}$ is the approximation to $\frac{\partial L(U)}{\partial U}$ and $U_{correction}$ is the correction value to U. There are many methods which can be used to solve this linear system. In this work, at each iteration we use a sparse GMRES implementation based upon [30], along with an under-relaxed version of (29) to improve robustness:

$$U = U + C_1 U_{correction}, \tag{34}$$

where C_1 is an under-relaxation factor (in this paper $C_1 = 0.2$).

In order to ensure that the force balance equation is satisfied, we update the reference thickness H_{00} as follows:

$$H_{00} \leftarrow H_{00} - C_2\left(\frac{2\pi}{3} - \sum_{e=1}^{N} \sum_{i=1}^{p^e+1} G_i^e u_i^e\right), \tag{35}$$

where C_2 is an under-relaxation factor for H_{00} ($C_2 = 0.1$ is used in this paper) and G_i^e is defined in (23). Although this update is decoupled from the solution of (27) in this work, it should also be possible to combine (35) with (27) to form a single nonlinear system.

Although the iterative solver described above does yield a solution of the discrete system of equations it often converges quite slowly. Conventional multigrid techniques are not appropriate for the acceleration of this convergence since the use of high order DG means that very few mesh elements are required. However, there is is a multi-level technique that is suitable for high-order DG methods: p-multigrid [9]. Rather than using different spatial grids at different levels, p-multigrid uses different polynomial orders but the same spatial grid. The low frequency modes and the high frequency modes correspond to the low-order components and the high-order components respectively. Consequently the low-order restrictions serve as "coarse" levels. Both high frequency errors and low frequency errors can be eliminated effectively by relaxing on both "fine" and "coarse" levels. For convenience, a brief introduction to the two-level full approximation scheme (FAS) is now provided.

Consider the following nonlinear system which results from a degree p FE discretization of a PDE:

$$\mathcal{L}^p(u^p) = f^p, \tag{36}$$

where u^p is the discrete solution vector for p^{th} degree piecewise polynomial on a given grid, $\mathcal{L}^p(u^p)$ is the associated nonlinear system and f^p is a source term ($f^p = 0$ on the finest level). The discrete residual is defined by:

$$r^p = f^p - \mathcal{L}^p(u^p). \tag{37}$$

Let $q < p$ and let u^q denote the coefficients of a coarse level q^{th} degree piecewise polynomial approximation. The two-level correction scheme is given as follows:

(1) Restrict the state and the residual to the coarse level:

$$u_0^q = \tilde{I}_p^q u^p, \tag{38}$$

$$r^q = I_p^q r^p. \tag{39}$$

(2) Solve the coarse grid problem:

$$\mathcal{L}^q(u^q) = f^q = \mathcal{L}^q(u_0^q) + r^q. \tag{40}$$

(3) Interpolate the correction from the coarse level to the fine level and correct the fine level state:

$$e^p = I_q^p(u^q - u_0^q), \tag{41}$$

$$u^p = u^p + e^p. \tag{42}$$

In the above I_p^q is the residual restriction operator and $\tilde{I}_p^q$ is the state restriction operator (which need not necessarily be the same) whilst I_q^p is the state prolongation operator. For the results described in this work we use a hierarchical basis (see [32]) and have therefore taken

$$I_q^p = \begin{bmatrix} I_q \\ \\ 0 \end{bmatrix} \quad \text{and} \quad I_p^q = \begin{bmatrix} I_q & 0 \end{bmatrix}, \tag{43}$$

where I_q is the $q \times q$ identity matrix. The definition of $\tilde{I}_p^q$ is a little more complex than that of I_p^q and is based upon the projection

$$\int_\Omega N_k^q \sum_{i=1}^{n(q)} u_i^q N_i^q d\Omega \;=\; \int_\Omega N_k^q \sum_{j=1}^{n(p)} u_j^p N_j^p d\Omega \qquad \text{for } k = 1, ..., n(q)\ , \tag{44}$$

where $\{N_i^q\}$ is the hierarchical basis (of dimension $n(q)$) for the polynomial space of degree at most q and $\{N_i^p\}$ is the hierarchical basis (of dimension

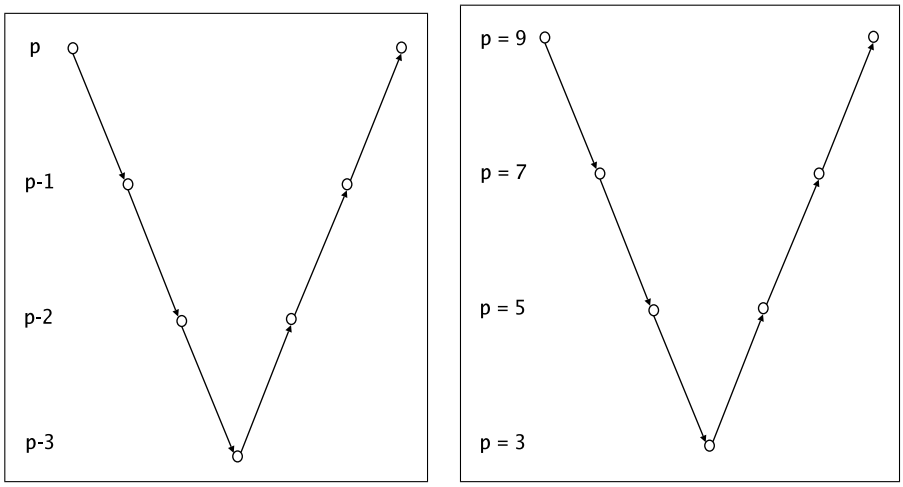

(a) $\triangle p = 1$ (b) $\triangle p = 2$

Fig. 2. Four level V-cycles for p-multigrid

$n(p)$) for the polynomial space of degree at most p. Full details may be found in [23].

This two-level scheme is easily extended to a multi-level version by applying the same scheme recursively to the solution of the coarse grid problem (40), using an even lower polynomial degree than q. Two four level examples are illustrated in Figure 2. In this figure $\triangle p$ represents the difference in order between consecutive levels of approximation, with $\triangle p = 1$ in Figure 2 (a) and $\triangle p = 2$ in Figure 2 (b). Unless otherwise stated, this latter scheme is used in all examples in this paper since our numerical tests indicate that it is more robust and efficient than other schemes considered. Note that our DG scheme is not stable for $p = 1$, [1,27].

5 Adaptivity

Since the solutions of typical EHL problems exhibit sharp local features, such as pressure spikes and rapid variations in the film thickness, some form of

adaptivity is essential for an efficient solution method. In this section we describe an adaptive algorithm based upon local h-refinement and coarsening, where the polynomial degree on each element is kept fixed. Of course it would also be possible to adapt the polynomial degree on each element too but this would significantly complicate the p-multigrid algorithm outlined in the previous section and would introduce issues associated with deciding between h- and p-refinement (see, for example, [10,21,22]). Furthermore, since the solution trial space is discontinuous over element interfaces, h-adaptivity is relatively easy to implement: unlike for C^0 finite elements which require continuity restrictions on element boundaries to be taken into account.

5.1 Adaptive Strategy

In [25], highly accurate one-dimensional solutions were obtained using an h-adaptivity method based on the magnitude of the high-order components of the solution on each element. In this paper, we extend this approach to the two-dimensional problems considered here. For the *hierarchical* basis functions [32] used in this paper, the high-order modes can be viewed as terms added to a lower order solution in order to improve its accuracy. To illustrate this we re-write equation (15), for the solution P^e on an element e, as:

$$P^e(X) = \sum_{i=1}^{n(p^e-d)} u_i^e N_i^e(X) + \sum_{i=n(p^e-d)+1}^{n(p^e)} u_i^e N_i^e(X). \tag{45}$$

Here the second sum contains only terms of the highest d polnomial orders, whilst the first sum contains the terms of order at most $p^e - d$. A simple error

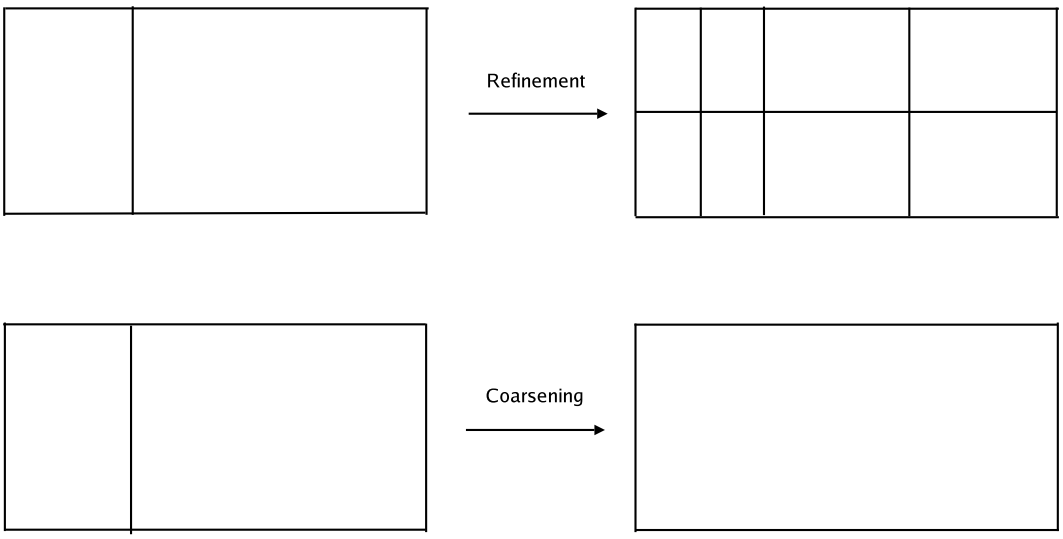

Fig. 3. H-adaptivity

indicator is provided by considering

$$E^e = \left\| \sum_{i=n(p^e-d)+1}^{n(p^e)} u_i^e N_i^e(X) \right\|_2 = \sqrt{\int_{\Omega_e} \left(\sum_{i=n(p^e-d)+1}^{n(p^e)} u_i^e N_i^e(X) \right)^2 \mathrm{d}X.}, \qquad (46)$$

where $d = 1$ or $d = 2$ are typically selected. The use of such an error indicator leads to the following rules for local mesh adaptivity.

(1) Refine element E if $E^E > Tol_1$, where Tol_1 is a given tolerance, by splitting E into 4 equally sized smaller elements (see Figure 3 (a)).
(2) Remove edge k, which has two neighbouring elements e and f, if $E^e < Tol_2$ and $E^f < Tol_2$, where Tol_2 is a smaller tolerance than Tol_1 (see Figure 3 (b)).

By following this approach the quality of the numerical solution can be ensured by the h-adaptivity which can make all of the highest-order components smaller than Tol_1.

Once the grid is adjusted, the current solution on the original grid needs to be transferred onto the new grid so that the computation may be continued from the current estimate of the solution. The two-dimensional data transfer between the new grid and the old grid includes two cases: transferring the solution from one original element to four equally sized smaller elements, and transferring the solution from two neighbouring smaller original elements to one new larger element which is generated by agglomerating these two elements. Thus, two local transfer operators, I_f^c and I_c^f, are required.

First we consider a transfer operator I_c^f to transfer solution from E to e_1, e_2, e_3 and e_4 (see Figure 3 (a)). This may be achieved through interpolation by enforcing

$$\int_{e_k} P^E(X) v \mathrm{d}X = \int_{e_k} P^{e_k}(X) v \mathrm{d}X, \ \forall v \in \{N_i^{e_k}(X), i = 1, 2, \ldots, n(p^{e_k})\}, \quad (47)$$

for $k = 1, 2, 3, 4$. Clearly the I_f^c operator cannot generally be an interpolant however it may be defined by enforcing the following weak form, which represents a local projection:

$$\int_E P^E(X) v \mathrm{d}X = \int_{e+f} P^{e+f}(X) v \, \mathrm{d}X, \ \forall v \in \{N_i^E(X), i = 1, 2, \ldots, n(p^E)\}. \quad (48)$$

Here $P^E(X) = \sum_{i=1}^{n(p^E)} u_i^E N_i^E(X)$ is the pressure in E and $P^{e+f}(X)$ is the pressure in $e + f$, where $P^{e+f} = P^e = \sum_{i=1}^{n(p^e)} u_i^e N_i^e(X)$ when $X \in e$ and $P^{e+f} = P^f = \sum_{i=1}^{n(p^f)} u_i^f N_i^f(X)$ when $X \in f$.

It should be noted that when adaptivity, and the data transfer to the new grid has taken place, it is also necessary to recompute the kernels in (21) for all ele-

ments, Ω_e, which have been introduced or modified by the adaptive procedure. This may be an expensive operation when the adaptivity is extensive.

6 Overall Solution Procedure

Having introduced all of the components of the solution algorithm, this section briefly describes how the p-multigrid may be combined with h-adaptivity to provide the following overall solution procedure.

1 Give an initial grid and ensure that this grid covers the pressurized domain. That is to say, the left boundary of the given grid is required to be far away from the contact centre and the actual cavitation position should be inside the given grid. Provide Tol_1 and Tol_2 for h-adaptivity.

2 Initialize the pressure on the given grid (for example, the Hertzian dry contact pressure profile [34] is used in this paper). Give an initial guess for H_{00}.

3 Calculate the kernels K_i^e (see equation (21)) at all quadrature points in element interiors and on element boundaries, and calculate the kernels G_i^e (see equation (23)).

4 Perform 1 or 2 p-multigrid V-cycles on the current grid to update the solution. On the initial grid, which is usually coarse, more V-cycles should be undertaken to make the solution almost converge. Note that H_{00} is only updated on the finest level.

5 Check if the grid needs to be adapted according to Tol_1 and Tol_2.

6 If the grid does need to be adapted: adapt the grid, transfer the current pressure profile from the old grid onto the new grid, calculate the kernels K_i^e and G_i^e related to the new elements, go to 4.

7 Perform further p-multigrid V-cycles until the L_2-norm of the numerical residual is less than 10^{-10}. Stop if $E^e < Tol_1$ for each element, else go to 6.

7 Numerical Results

7.1 Lightly loaded EHL solutions

We begin this section by presenting representative results for three lightly loaded test cases: (a) $W = 0.2 \times 10^{-7}$, $U = 0.1 \times 10^{-11}$ and $G = 5000$; (b) $W = 0.6 \times 10^{-7}$, $U = 0.15 \times 10^{-11}$ and $G = 5000$; (c) $W = 0.7 \times 10^{-7}$, $U = 0.3 \times 10^{-11}$ and $G = 5000$ (see (7)-(10)). There is nothing special about these particular cases other than that they show solutions for a selection of lightly-loaded EHL cases. For each case, the same initial guess is used: $H_{00} = 0$ with the piecewise bilinear interpolant of the Hertzian dry contact pressure profile,

$$p(x,y) = \begin{cases} \sqrt{1-x^2-y^2} & \text{if } |x^2+y^2| < 1 \\ 0 & \text{otherwise} \end{cases}. \tag{49}$$

This initial guess is shown in Figure 5 for a typical initial grid (see Figure 4). Note that the initial pressure profile is not smooth, and discontinuities over the element boundaries can be observed. Of course, a smoother initial guess could be more suitable but this choice of initial data demonstrates that a good initial guess is not generally required for these lightly-loaded cases.

For these results, values of $d = 1$, $Tol_1 = 0.001$ and $Tol_2 = 0.00005$ are used for the h-adaptivity and polynomial degree 9 is used in each element. On the initial grid, 10 V-cycles are performed to resolve an almost converged solution prior to any h-adaptivity. After the first h-adaptivity, the quality of the current

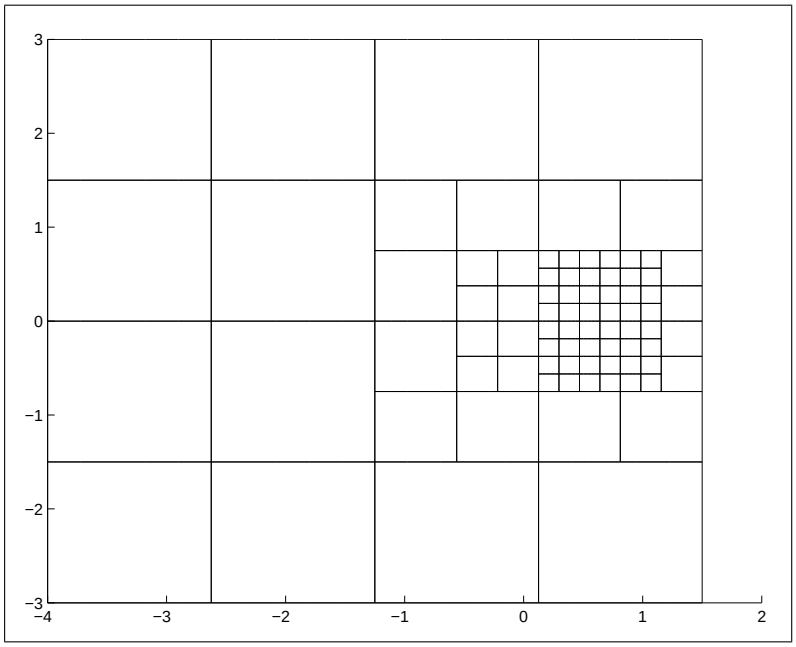

Fig. 4. Initial grid

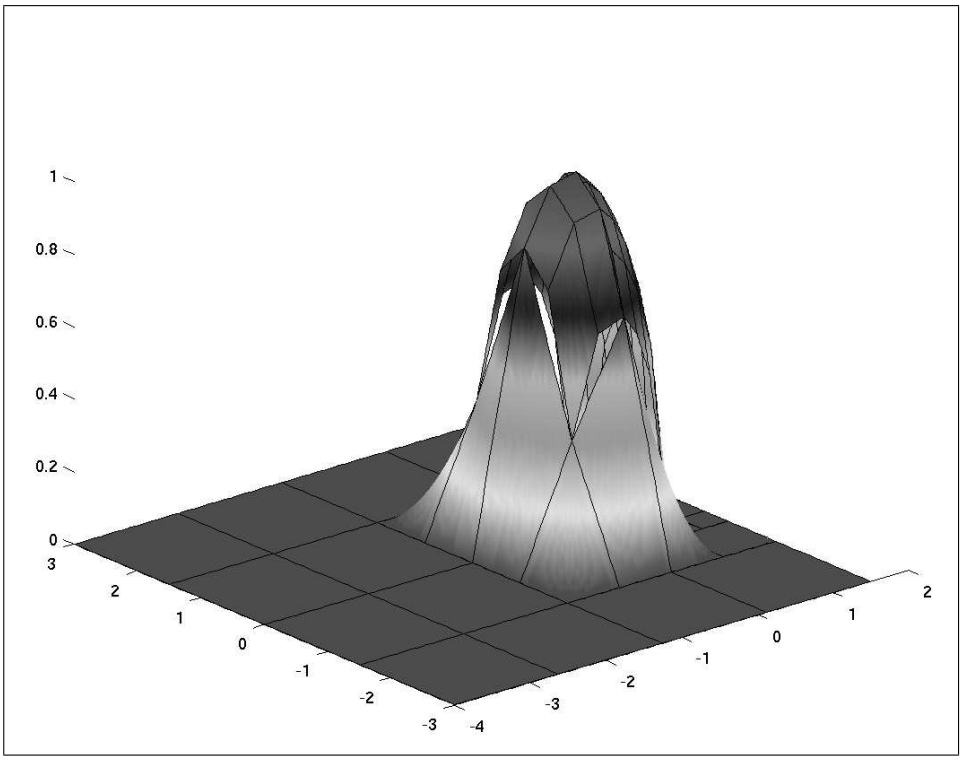

Fig. 5. Initial pressure profile

solution is checked after every 2 V-cycles before repeated h-adaptivity until the quality of the solution is satisfactory ($E^e < Tol_1$ for each element e) and fully converged (the L_2-norm of the numerical residual is less than 10^{-10}).

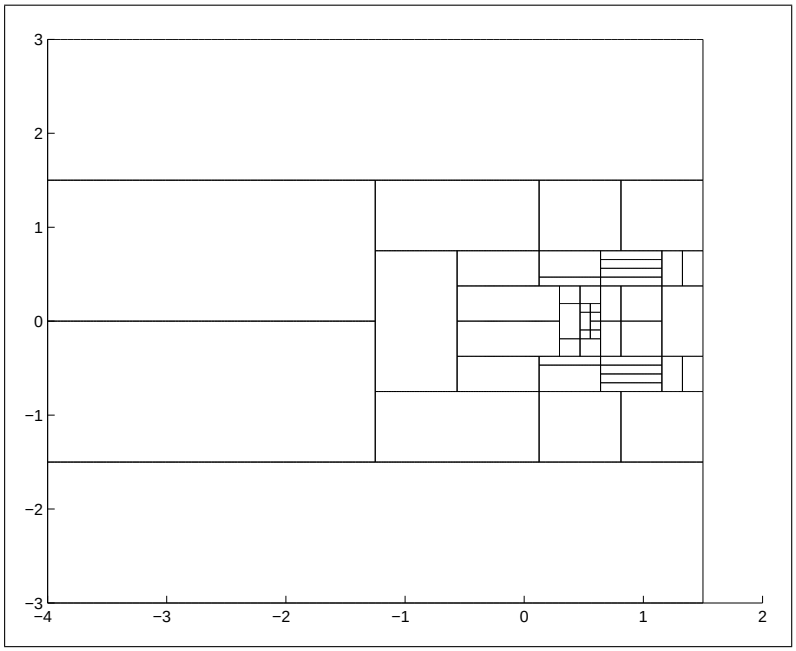

Fig. 6. Final grid (a): $W = 0.2 \times 10^{-7}$, $U = 0.1 \times 10^{-11}$ and $G = 5000$

The final grids generated in these three cases are displayed in Figure 6, 8 and 10, where the mesh size around the pressure ridge is much smaller than in other regions. The total number of elements required in each case is 48, 114 and 246 respectively. The fully converged pressure profiles for each of these cases are displayed in Figures 7, 9 and 11 respectively (note that use of DG with $p = 9$ corresponds to 57 degrees of freedom on each element). In each case a smooth pressure profile is obtained and the pressure ridge, which characterizes point contact EHL problems, is accurately captured. To obtain similar resolution using existing finite difference or continuous finite element approaches requires much larger numbers of degrees of freedom (see, for example, [34,11,12] or [14,16] respectively).

For all three of these cases, P increases smoothly from the inflow boundary ($x = -4.0$) to the contact centre ($x = 0, y = 0$) along the central line $y = 0$. The pressure then drops a little before rising steeply to the top of the pressure ridge. In the short distance between the top of the pressure ridge and the

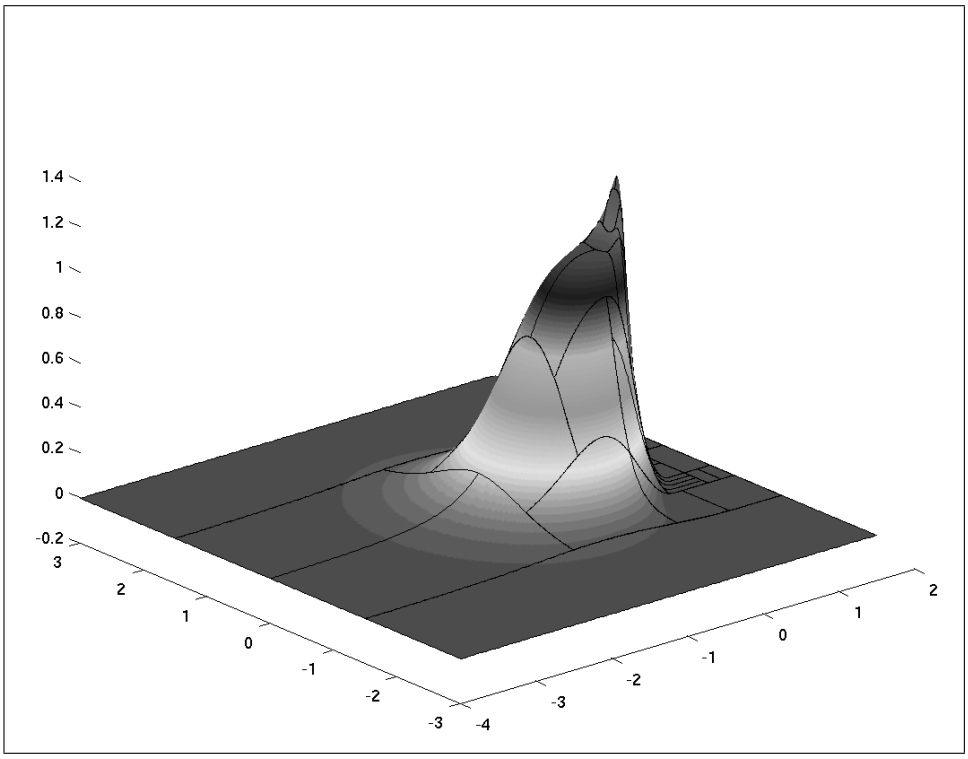

Fig. 7. Converged pressure profile (a): $W = 0.2 \times 10^{-7}$, $U = 0.1 \times 10^{-11}$ and $G = 5000$

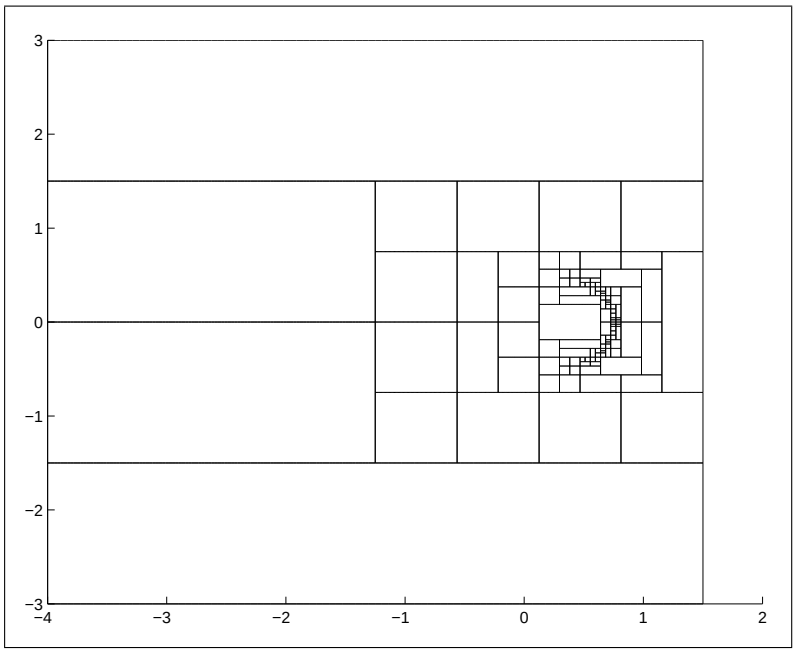

Fig. 8. Final grid (b): $W = 0.6 \times 10^{-7}$, $U = 0.15 \times 10^{-11}$ and $G = 5000$

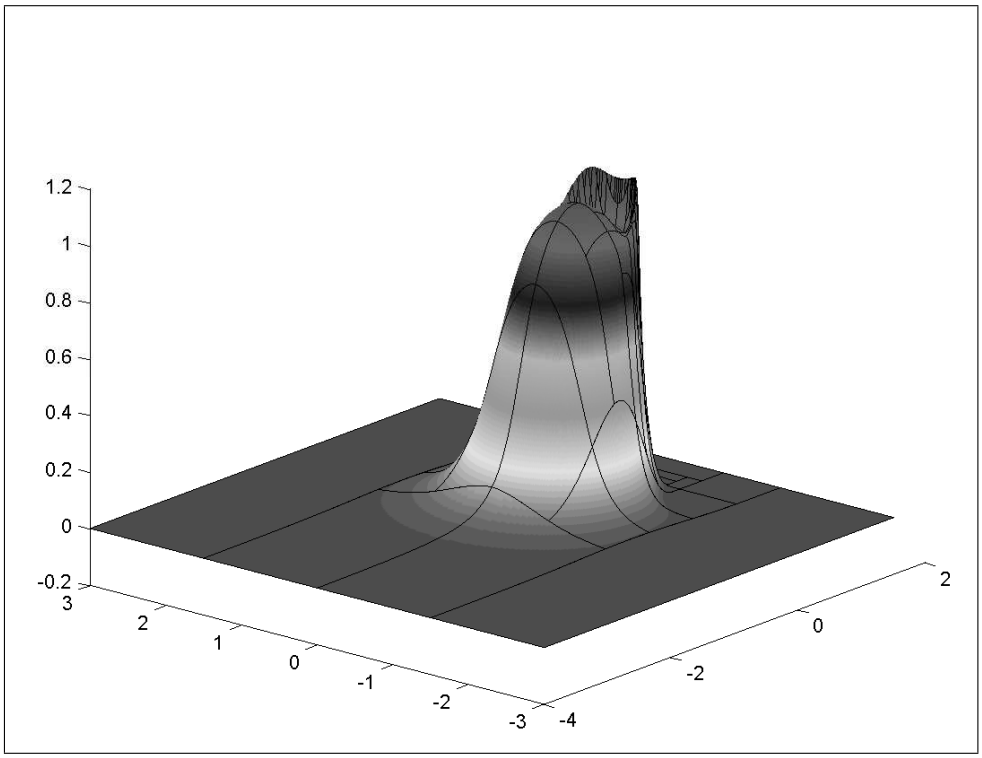

Fig. 9. Converged pressure profile (b): $W = 0.6 \times 10^{-7}$, $U = 0.15 \times 10^{-11}$ and $G = 5000$

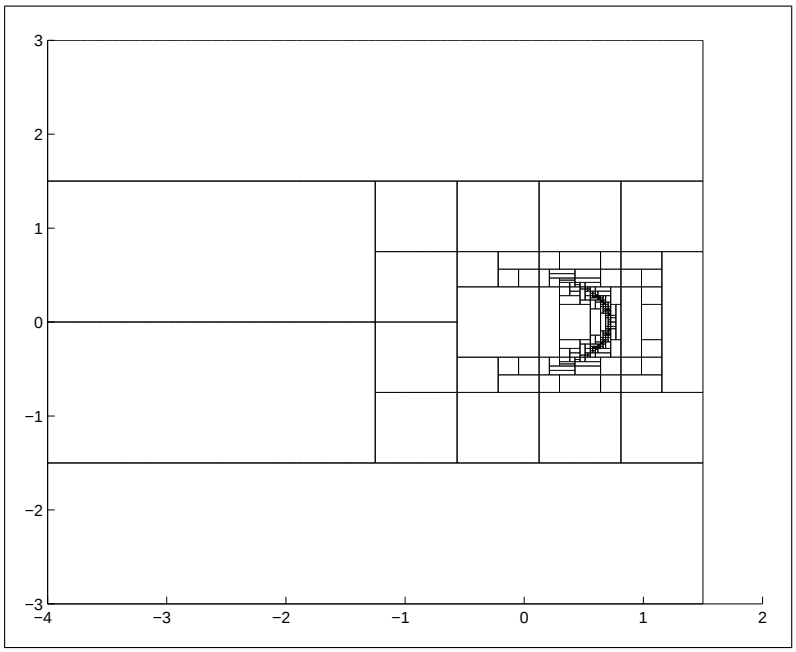

Fig. 10. Final grid (c): $W = 0.7 \times 10^{-7}$, $U = 0.3 \times 10^{-11}$ and $G = 5000$

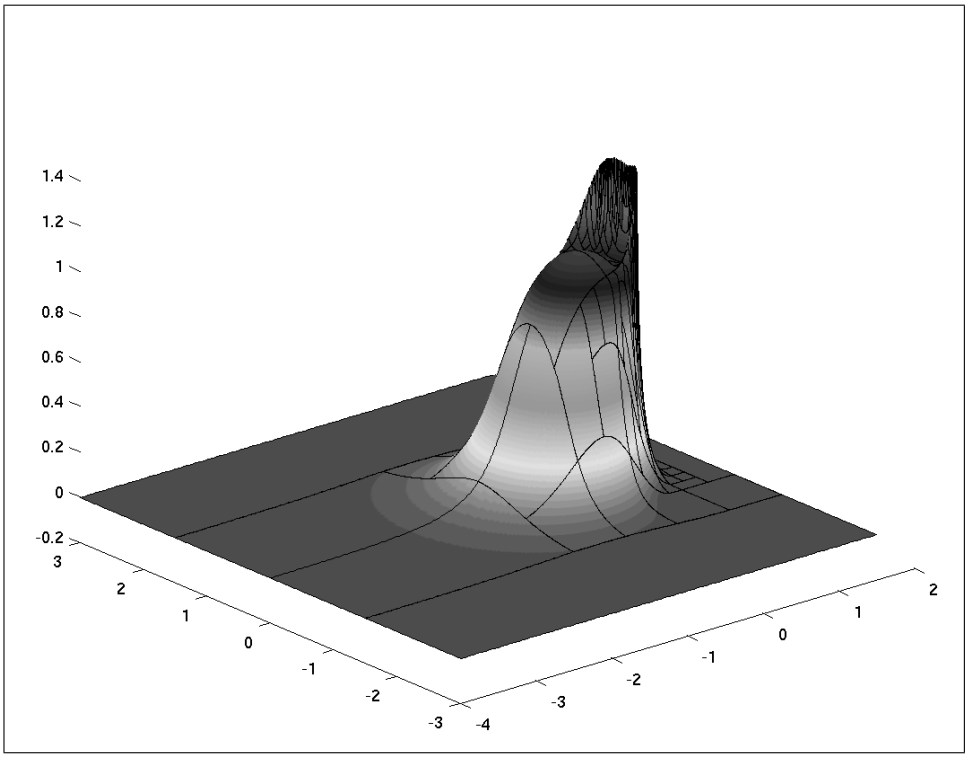

Fig. 11. Converged pressure profile (c): $W = 0.7 \times 10^{-7}$, $U = 0.3 \times 10^{-11}$ and $G = 5000$

cavitation boundary, where P becomes zero, the pressure decreases rapidly. It should be noted however that the shapes of these three pressure ridges are significantly different. In Figure 7 (the lightest load), the maximum pressure is located on the central line $y = 0$ and P decreases in both the x and y directions from the top of the pressure ridge. In Figures 9 and 11 however, the maximum pressure is not on the central line (and so, due to symmetry, there are in fact two maxima). In Figure 9, for example, the pressure at the top of the ridge increases significantly from the central line when moving in the y and $-y$ directions, before decreasing rapidly to zero. These solutions are reproducible for different choices of p, d, Tol_1 and Tol_2 (with different numbers of elements in the final grids of course). Consequently, we have also been able to demonstrate that the adaptive high order DG method can yield accurate solutions to very challenging EHL problems using remarkably few

degrees of freedom ((a) 48×57, (b) 114×57 and (c) 246×57). Furthermore, the approach behaves in a stable manner.

7.2 More heavily loaded cases

The three cases shown above consider loading up to p_H=343MPa. For many industrial scenarios requiring EHL modelling the loading exceeds this, despite the overall solutions still resembling those for case (c). In this section we present two more heavily loaded cases, and discuss some of the issues that affect the computation of accurate solutions. These cases are (d) $W = 1.63 \times 10^{-7}$, $U = 0.818 \times 10^{-11}$ and $G = 4972$; (e) $W = 4.63 \times 10^{-7}$, $U = 0.818 \times 10^{-11}$ and $G = 4972$, which have significantly higher W and U values than cases (a) to (c). The maximum Hertzian pressure for these cases is 450MPa and 637MPa respectively. Case (d) is equivalent to the M=20, L=10 test case used in [11] and is almost identical that used by Venner and Lubrecht [35].

In order to get convergence of the solver on these higher loaded cases we have found it necessary to use continuation solutions from lighter loaded cases as an initial guess. This method is common for accelerating convergence in many EHL cases, e.g. [13]. An important consideration when using continuation is that the initial grid should not be too refined to match the pressure ridge since the increase in pressure will significantly affect its location. It is also necessary to reduce the relaxation parameters used in order to improve the robustness of the solver.

The solutions presented in this section use $p = 7$ polynomials giving 38 unknowns per element. The adaptivity strategy used is exactly the same as that

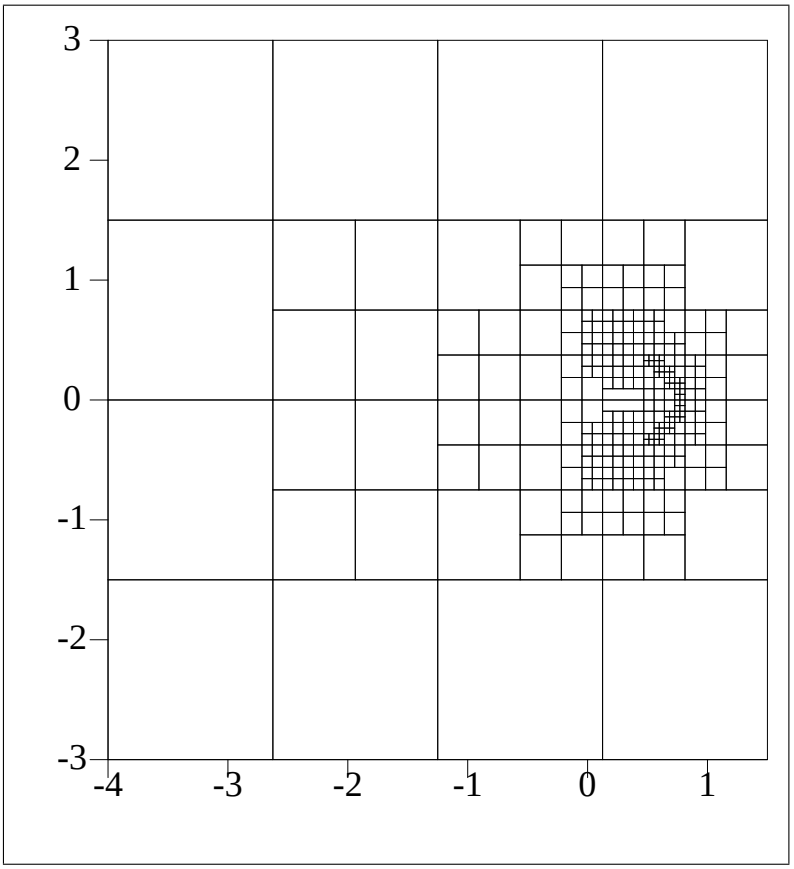

Fig. 12. Final grid (d): $W = 1.63 \times 10^{-7}$, $U = 0.818 \times 10^{-11}$ and $G = 4972$

described for the lightly loaded cases. The final meshes for cases (d) and (e) are shown in Figures 12 and 14. They contain 292 and 232 elements respectively. The fully converged pressure solutions are shown in Figures 13 and 15. It can be clearly seen that as the cases get more heavily loaded, more resolution is needed around the whole outflow side of the pressure bump, and also in the inlet region.

For these heavily loaded cases it does seem that convergence becomes much harder to achieve. This seems to mainly be caused by the difficulties of accurately resolving the pressure ridge formed against the back of the main pressure bump using the high order polynomials chosen. This is demonstrated for cases (d) and (e) in Figure 16. In can be seen how, as the load gets heav-

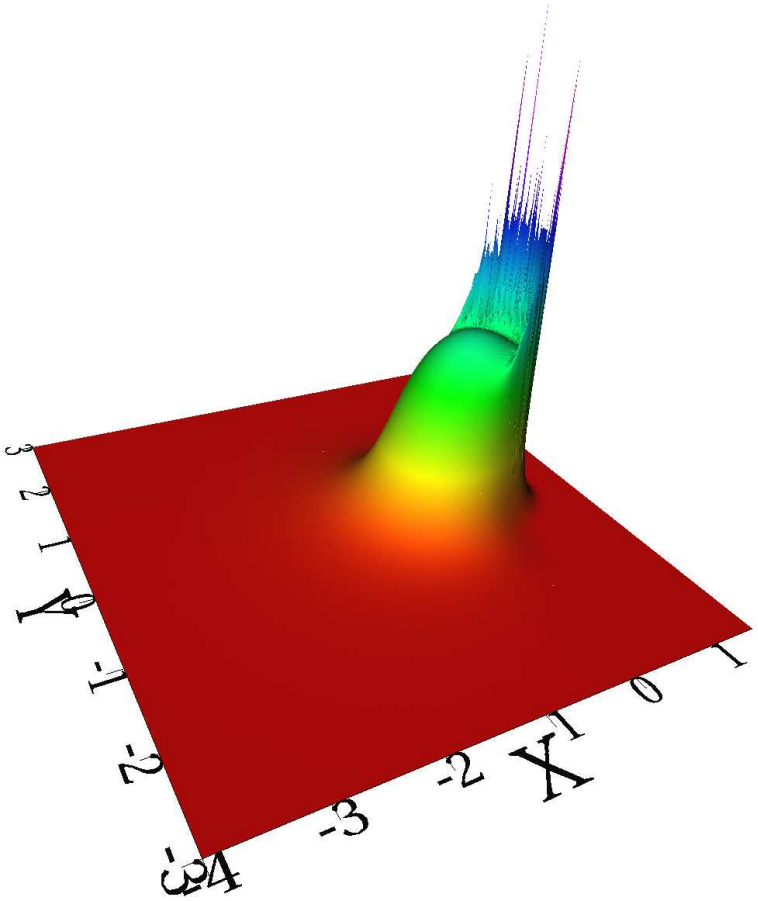

Fig. 13. Converged pressure profile (d): $W = 1.63 \times 10^{-7}$, $U = 0.818 \times 10^{-11}$ and $G = 4972$

ier, the pressure ridge gets narrower and hence harder to resolve. This also contributes to the jaggedness of the top of the pressure ridge in the visualisza-tions shown in Figures 13 and 15. In these cases the elements which partially contain the ridge have a "waviness" effect evident away from the ridge in what should be an area of smooth solution variation.

7.3 Efficiency and robustness

The numerical results above show that accurate solutions can be obtained, at least for light to moderate loads, using a relatively small number of degrees of

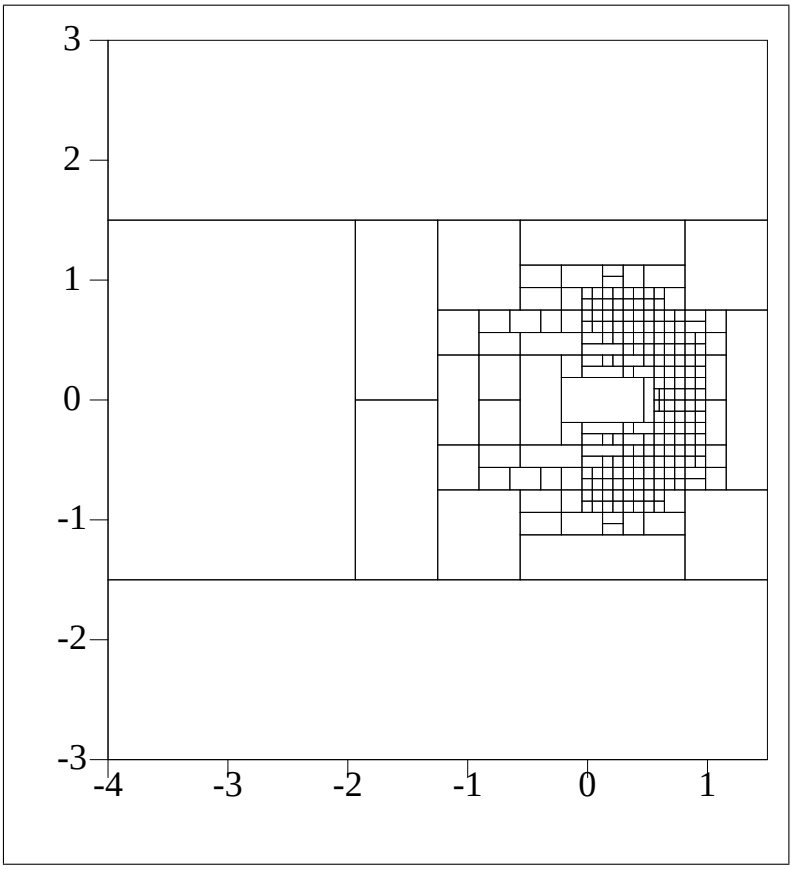

Fig. 14. Final grid (e): $W = 4.63 \times 10^{-7}$, $U = 0.818 \times 10^{-11}$ and $G = 4972$

freedom. In particular, the typical pressure ridges that occur in these lightly loaded cases can be precisely resolved. For more highly loaded cases it is likely that the approach would be enhanced by the capability of applying adaptivity in the polynomial degree as well as the element size (i.e. full h-p-adaptivity). This is because the high order polynomials are less well suited to capturing extremely narrow pressure ridges than lower order polynomials would be on very fine meshes. Hence the ideal finite element representation would have high order elements almost everywhere but lower order elements in the precise vicinity of the narrow pressure ridge.

The cost of the method, in terms of both memory and computation time, is dominated by the evaluation of the film thickness, (20) and (21). This is made

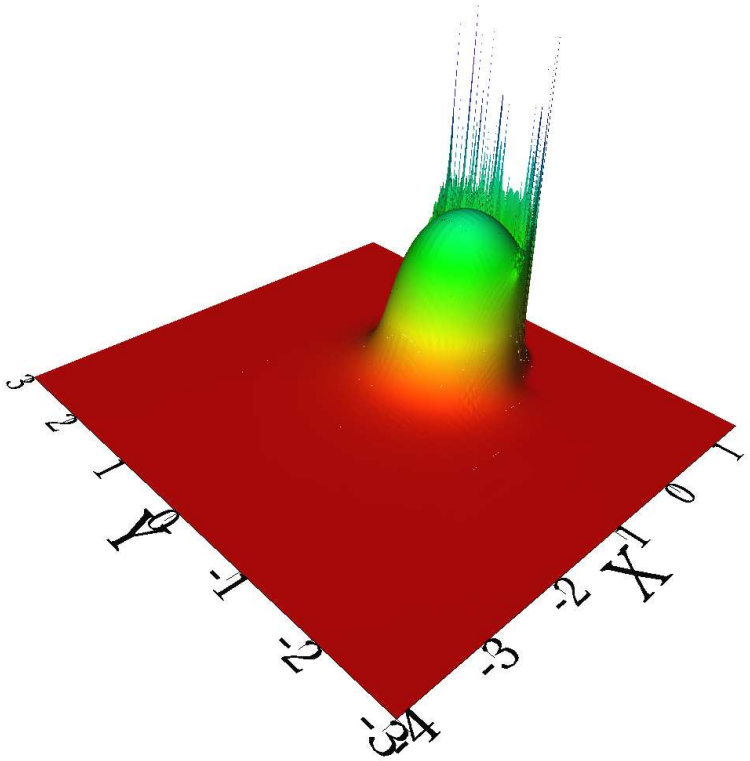

Fig. 15. Converged pressure profile (e): $W = 4.63 \times 10^{-7}$, $U = 0.818 \times 10^{-11}$ and $G = 4972$

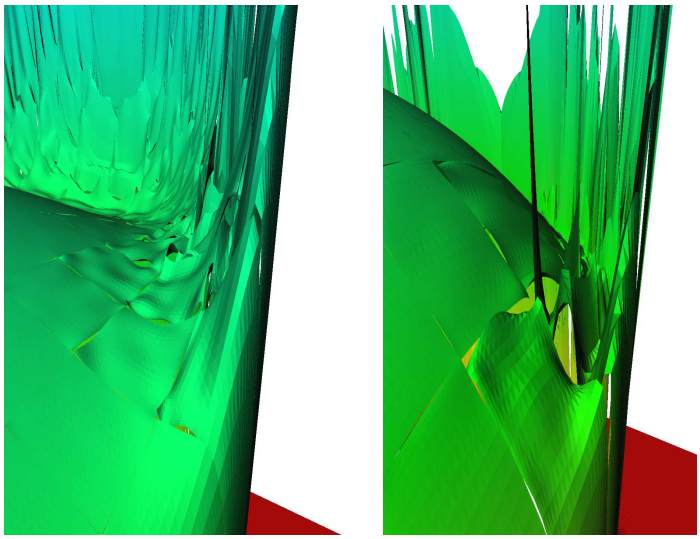

Fig. 16. Zoom of the pressure ridge for cases (d), left, and (e), right.

tractable due to the precomputation of the kernel functions (21) at quadrature points, however the computation of these kernels is still relatively expensive compared to the overall solution time, especially when mesh adaptivity is used due to the need to recompute kernels after each mesh adaptation. For example, for the lightly loaded case (b) above, involving 6498 degrees of freedom, it costs 62098 seconds to obtain the fully converged solution of which 51150 seconds are spent on the calculation of these kernels. An alternative approach, that may be worthy of consideration therefore, could be to use a fixed mesh that is chosen in advance using our *a priori* knowledge of the qualitative pressure profiles. Note that, as currently implemented, our solution time for case (b) is comparable to that required to solve a similar problem to a similar accuracy (on a 16385×16385 finite difference grid for example) using a state-of-the-art lower order scheme, [12]. However one would be unlikely to use such a fine finite difference grid for a problem with this load in practice. Hence, whilst the DG approach requires substantially less memory (even allowing for the precomputation of the kernel functions), the finite difference solver is applicable with lower resolution and has been shown to extend much more effectively to highly loaded cases than the DG approach used here. Of course, there have been many years of development to improve the efficiency of lower order implementations whereas our DG implementation is a new development for this problem and is therefore likely to benefit from further research.

It may be observed that in the presentation of the algorithm described above there are a number of parameters that must be selected. It is approproate therefore to give some consideration to the choice of these parameters and to the sensitivity (or otherwise) of the computed results to such parameter values. The first parameter that we consider is Tol_1, which is used in order to

Table 1

Comparison of Pressure Peak Position and Peak Pressure

Tol_1	Number of Elements	Peak Pressure	Peak Position
0.025	26	1.333	(0.576,0.000)
0.005	34	1.324	(0.578,0.000)
0.001	48	1.322	(0.579,0.000)
0.0002	89	1.320	(0.578,0.000)

control the local h-refinement. In addition to the value of $Tol_1 = 0.001$ that is used above, the loaded case (a) is also solved using three other tolerances: $Tol_1 = 0.025$, $Tol_1 = 0.005$ and $Tol_1 = 0.0002$ respectively. Table 1 shows a detailed comparison of the peak pressures and the peak positions when using these different Tol_1 values. It is apparent that no significant difference can be observed when $Tol_1 < 0.005$ and so one may conclude that $Tol_1 = 0.001$ is sufficiently cautious to ensure an accurate solution and that the results are not sensitive to a variation in this parameter once it is sufficiently small.

For the loaded case (a), another numerical test is performed to assess the sensitivity of the solution to the choice of the polynomial degree p. Here we use different orders ($p = 3, 5, 7, 9$) on the same grid, which is generated using the h-adaptivity when $p = 9$. The comparison of the pressure peak profiles along $Y = 0$ is shown in Figure 17. When $p = 3$, significant discontinuities can be observed. With $p = 5$ the discontinuities become smaller, but may still be observed. When $p >= 7$, the pressure ridges are much smoother and no significant difference can be observed between the results. Finally, Table 2 illustrates that the peak pressure value and position is only accurately repre-

Table 2

Comparison of Pressure Peak Position and Peak Pressure

p	Peak Pressure	Peak Position
3	1.156	(0.578,±0.009)
5	1.317	(0.583,±0.004)
7	1.321	(0.581,0.000)
9	1.322	(0.580,0.000)

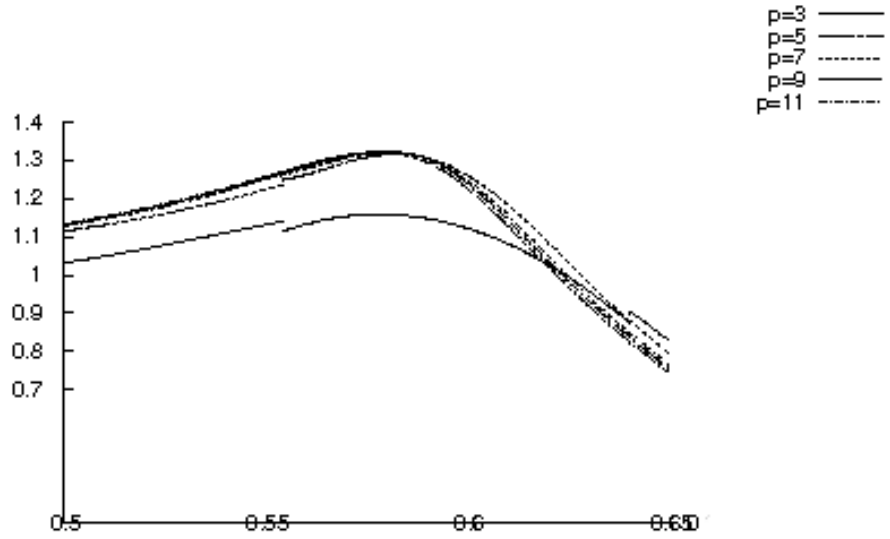

Fig. 17. Comparison of the pressure peak profiles along $Y = 0$ on the same grid with different orders

sented for $p >= 7$ on this particular grid. Of course, these sensitivity tests are reported here for one of the lightly loaded cases. For the more heavily loaded cases discussed in cases (d) and (e) the best choice of parameters to ensure both accuracy and robust convergence is less clear.

8 Discussion

In this paper a high-order finite element scheme, based upon the Discontinuous Galerkin method, has been successfully applied to a selection of two-dimensional EHL contact problems. This is the first time that the feasibility of the DG approach has been demonstrated for such problems and it successfully extends the previous one-dimensional work of [24]. In order for the approach to be of practical value it is clear that it must be computationally competitive when contrasted with existing solution methods based upon lower order schemes (as in [12,34,36] for example) or based upon continuous finite elements (e.g. [8,14,15]. In order to facilitate this a suitable p-multigrid solver has been developed, which incorporates a robust smoother in both the contact and the non-contact regions. Furthermore, in order to capture all details of the EHL solutions, particularly the pressure ridge, an h-adaptivity method has been implemented with refinement and coarsening controlled via a flexible error indicator function. In the examples included in this paper this function is based upon the significance of the highest-order contributions to the DG solution however alternative controls are also possible, and have been implemented, based upon the jumps in the DG solution for example [23]. It should be acknowledged however that, even with these enhancements to the solution strategy the CPU requirements of our initial implementation are very substantial compared to more traditional methods. It is also important to acknowledge that, as presented here, the high order DG approach has not performed well for highly loaded cases. It has not been possible to obtain converged solutions for higher loaded cases than those reported here, and even in the moderately loaded cases (d) and (e) the solutions obtained are not smooth across the

pressure ridge.

There are a number of possibilities for enhancing the performance, both in terms of speed and robustness, that will need to be investigated further if the DG approach is to be widely applicable to the solution of these problems. For example, in this work we have adopted the relatively straightforward approach of selecting a polynomial degree *a priori* and then adding and deleting degrees of freedom via the use of h-adaptivity. Clearly, an hp-adaptive approach, [21], offers significantly greater versatility however an effective and reliable technique is required for selecting which type of refinement or coarsening is required at any given point in time and space. If such a technique can be found however the hp-adaptive approach offers substantial further efficiency gains. Additional efficiency benefits may also be obtained by successfully parallelizing the method, since the high order DG is well suited to parallel implementation [3], and the computation of each of the kernels is independent of all others. Indeed, the kernel evaluations is by some way the most expensive component of the solution process.

Further improvements might be possible by enhancing the quasi-Newton iteration that lies at the heart of the solution process. For example, the approximation to the Jacobian matrix could be improved significantly for highly-loaded problems and/or in regions of local h-refinement. It should also be possible to couple equations (35) and (27) to form a single nonlinear system. An alternative direction in which to take this work would be to drop the integral form (3) for the film thickness altogether and to follow the approach of [14] by computing a finite element approximation to the elastic deflection and coupling this to the DG discretization of the Reynolds equation within one over-arching nonlinear system. Given the significant advantages that have been reported

for this fully-coupled approach, [14,16,17], this seems a particularly attractive option. A final generalization of the software that is also highlighted here for future consideration is the solution of transient point contact problems, involving variable loads or roughness in the contacting elements.

References

[1] C.E. Baumann, J.T. Oden, A discontinuous hp finite element method for convection-diffusion problems. *Comput. Methods Appl. Mech. Engrg.*, 175:pp311–341, 1999.

[2] A. Brandt, A.A. Lubrecht, Multilevel matrix multiplication and fast solution of integral equations. *J. Comput. Phys*, 90:pp348–370, 1990.

[3] B. Cockburn, G.E. Karniadakis, C.W. Shu, *Discontinuous Galerkin Methods: Theory, Computation and Applications. Springer-Verlag*, Berlin, 1999.

[4] D. Dowson, *Biotribology.* Professional Engineering Publishing, 2005.

[5] D. Dowson, G.R. Higginson, A numerical solution to the elasto-hydrodynamic problem. *Journal of Mechanical Engineering Science*, 1(1):pp6–15, 1959.

[6] C.D. Elcoate, H.P. Evans, T.G. Hughes, On the coupling of the elastohydrodynamic problem. *Proc. Instn Mech. Engrs. Part C.*, 212:pp307–318, 1998.

[7] E. Evans, *Practical Numerical Integration.* WILEY, 1993.

[8] H.P. Evans, T.G. Hughes, Evaluation of deflection in semi-infinite bodies by a differential method. *Proc. Instn Mech. Engrs. Part J.*, 214:pp563–584, 2000.

[9] K.J. Fidkowski, D.L. Darmofal, Development of a higher-order solver for aerodynamic applications. *42nd AIAA Aerospace Sciences Meeting and Exhibit,*

AIAA Paper., Jan, 2004.

[10] J.D. Frazier, P.K. Jimack, R.M. Kirby, On the use of adjoint-based sensitivity estimates to control local mesh refinement. *Comm. Comp. Phys.*, 7:pp631–638, 2010.

[11] C.E. Goodyer, *Adaptive Numerical Methods for Elastohydrodynamic Lubrication*. PhD thesis, University of Leeds, Leeds UK, 2001.

[12] C.E. Goodyer, M. Berzins, Parallelization and scalability issues of a multilevel elastohydrodynamic lubrication solver. *Concurrency and Computation: Practice and Experience*, 19(4):pp369–396, 2007.

[13] C.E. Goodyer, R. Fairlie, D.E. Hart, M. Berzins, L.E. Scales, Calculation of friction in steady-state and transient EHL simulations. *Transient Processes in Tribology: Proceedings of the 30th Leeds-Lyon Symposium on Tribology, Elsevier*, 2004.

[14] W.Habchi, *A Full-System Finite Element Approach to Elastohydrodynamic Lubrication Problems: Application to Ultra-Low-Viscosity Fluids*. PhD thesis, INSA de Lyon, France, 2008.

[15] W. Habchi, I. Demirci, D. Eyheramendy, G. Morales-Espejel, P. Vergne, A finite element approach of thin film lubrication in circular EHD contacts. *Tribology International*, 40:pp1466–1473, 2007.

[16] W. Habchi, D. Eyheramendy, P. Vergne, G. Morales-Espejel, A full-system approach of the elastohydrodynamic line/point contact problem. *Journal of Tribology - Trans. ASME*, 130:021501, 2008.

[17] W. Habchi, D. Eyheramendy, P. Vergne, G. Morales-Espejel, Stabilized fully-coupled finite elements for elastohydrodynamic lubrication problems. *Advances in Engineering Software*, in press.

[18] D. Hart, M. Berzins, C.E. Goodyer, P.K. Jimack, Using adjoint error estimation techniques for elastohydrodynamic lubrication line contact problems. *Int. J. Numer. Meth. Fluids*, in press.

[19] T.G. Hughes, C.D. Elcoate, H.P. Evans, A novel method for integrating first and second order differential equations in elastohydrodynamic lubrication for the solution of smooth isothermal, line contact problems. *International Journal for Numerical Methods in Engineering*, 44:pp1099–1113, 1999.

[20] C.C. Kweh, H.P. Evans, R.W. Snidle, Elastohydrodynamic Lubrication of heavily loaded circular contacts. *Proc. Instn. Mech. Engrs. Part C*, 203:pp133–148, 1989.

[21] E.J. Kubatko, J.J. Westerink, C. Dawson, Hp discontinuous Galerkin methods for advection dominated problems in shallow water flow *Comput. Methods Appl. Mech. Engrg.*, 192:pp.437–451, 2006.

[22] J. Kurtz, L. Demkowicz, A fully automatic hp-adaptivity for elliptic PDEs in three dimensions. *Comput. Methods Appl. Mech. Engrg.*, 196:3534–3545, 2007.

[23] H. Lu, *High Order Finite Element Solution of Elastohydrodynamic Lubrication Problems*. PhD thesis, University of Leeds, UK, 2006.

[24] H. Lu, C.E. Goodyer, M. Berzins, P.K. Jimack, High order Discontinuous Galerkin method for EHL line contact problems. *Comm. Num. Meth. Eng.*, 21:pp.643-650, 2005.

[25] H. Lu, M. Berzins, C.E. Goodyer, P.K. Jimack, M. Walkley, Adaptive high-order finite element solution of transient elastohydrodynamic lubrication problems. *Proc. IMechE Part J: J. Engrg. Tribology*, vol.220, pp.215-225, 2006.

[26] W.E. Lubrecht, A.A. ten Napel, R. Bosma, Multigrid, an alternative method for calculating film thichness and pressure profiles in elastohydrodynamically lubricated line contacts. *ASME, JOT*, 108:pp551–556, October 1986.

[27] I. Oden, J.T. Babuska, C.E. Baumann, A discontinuous hp finite element method for diffusion problems. *J. Comput. Phys.*, 146:pp495–519, 1998.

[28] A.I. Petrusevich, Fundamental conclusions from the contact-hydrodynamic theory of lubrication. *Izv. Akad. Nauk. SSSR (OTN)*, 2:pp209, 1951.

[29] O. Reynolds, On the theory of lubrication and its application to Mr Beauchamp Tower's experiments, including an experimental determination of the viscosity of olive oil. *Phil. Trans. R. Soc.*, 177:pp551–556, 1886.

[30] Y. Saad, M.H. Schultz, GMRES – A generalized minimal residual algorithm for solving non-symmetric linear systems. *SIAM J. Sci. Stat. Comp.*, 7:pp856–869, 1986.

[31] T.A. Stolarski, *Tribology in Machine Design*. Elsevier, 1990.

[32] B. Szabo, I. Babuska. *Finite Element Analysis*. Wiley, New York, 1991.

[33] C.H. Venner, Higher-order multilevel solvers for the EHL line and point contact problem. *ASME, JOT*, 116:pp741–750, October 1994.

[34] C.H. Venner, *Multilevel Solution of the EHL Line and Point Contact Problems*. PhD thesis, University of Twente, Endschende, The Netherlands, 1991.

[35] C.H. Venner, A.A. Lubrecht *Multilevel Methods in Lubrication*. Elsevier, 2000.

[36] J. Wang, S.Y. Qu, P. Yang, Simplified Multigrid Technique for the Numerical Solution to the Steady-State and Transient EHL Line Contacts and the Arbitrary Entrainment EHL Point Contacts. *Tribology International*, 34:pp191–202, 2001.

[37] S.R. Wu, A penalty formulation and numerical approximation of the Reynolds-Hertz problem of elastohydrodynamic lubrication. *Internat. J. Engrg. Sci.*, 24(6):pp1001–1013, 1986.